Influence of the ratio of nozzle inlet to nozzle throat areas on the performance of a jet pump for vacuum applications using computational fluid dynamics

Jose Alfredo Palacio, Ivan Patino and William Orozco

Abstract— **The nozzle design is one of the most important issues because it determines the pressure range and the other dimensions to guarantee an adequate performance of a jet_pump. An incorrect design of this part can cause shock waves and unnecessary overexpansion of the power fluid. The nozzle's main purpose is to allow the high-pressure, low-velocity primary fluid to be accelerated in such a way as to substantially decrease the fluid pressure while increasing its velocity. This is achieved because the subsonic flow accelerates when entering the convergent part of the nozzle, obtaining a sonic or supersonic flow at the nozzle throat that accelerates even more when entering the divergent part of the nozzle. Therefore, to achieve the highest possible nozzle discharge velocity, the nozzle must be able to change the flow conditions from subsonic to supersonic. Considering the high importance of the nozzle design in the jet_pump performance, five cases are simulated in the present work, where the ratio of nozzle inlet to nozzle throat areas is modified (10,15,20,25 y 30), to study the behavior of three performance parameters, namely, drag coefficient (Cd), pressure ratio (PR) and Energy Efficiency (η), as well as the Mach number (Ma) and velocity fields.**

Index Terms— **Computational Fluid Dynamics, Jet pump performance, Area ratio, Drag coefficient, Pressure ratio, Energy efficiency.**

I. INTRODUCTION

THE jet pumps operate under Bernoulli's principle where a high-pressure primary fluid undergoes a Venturi effect when it goes through a convergent-divergent nozzle, originating a suction of secondary fluid. In the present work, the k-ε turbulence model is used for the calculations, in which the turbulent viscosity is considered, as can be observed in Section B of Methodology.

Jose Alfredo Palacio, Pascual Bravo University
Email: josealpa@pascualbravo.edu.co

Ivan Patino, Pascual Bravo University
Email: i.patinoar@pascualbravo.edu.co

William Orozco, Pascual Bravo University
Email: william.orozco@pascualbravo.edu.co

Jet pumps have advantages such as their simplicity of construction, high reliability, geometric simplicity, small size, low cost of maintenance and acquisition, and wide range of operation. In a jet jump, the primary fluid enters the nozzle inlet at high pressure and low speed and then accelerates as it passes through the throat of the nozzle, reducing its pressure, thus generating a vacuum that allows the suction of another fluid called secondary.

In Fig. 1, the parts, geometry and basic operation of a jet pump are shown. According to [1]; when the fluid reaches sonic velocity at the nozzle throat (Pg in Fig1), supersonic velocity can be achieved at the outlet (P2) as long as the area ratio between the inlet and the nozzle throat is the adequate one, which leads to a higher pressure drop and, consequently, to a higher drag coefficient for the secondary fluid.
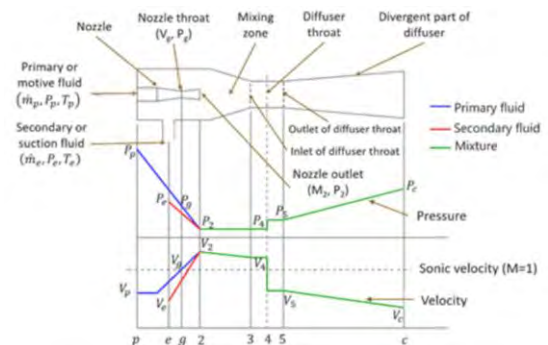

Fig. 1. Operation of a jet pump

The mixing zone in a jet pump was experimentally observed in [2] using an optical method, which allows precise observation of the mixing of two high-velocity flows combining Rayleigh scattering analysis, laser-induced fluorescence, and image

processing. In recent times, the entrainment and mixing phenomena of fluids in jet pumps were analyzed by [3] using computational fluid dynamics (CFD), concluding that the position of the nozzle outlet has a great influence on the critical backpressure and on the drag, coefficient produced by the device.

The position of the nozzle and its geometry also have a great influence on these phenomena, as demonstrated by [4], [5] using CFD; the maximum drag coefficient obtained in these works was 0.5. On the other hand, [6] performed CFD simulations for the transport of particulate matter in jet pumps using a Eulerian-LaGrange approach, where various fluid densities were considered, and the mass flow rate and fluid flow velocity from the dispersed phase to the nozzle outlet.

The most important contribution of [7] was the study on the blocking condition conditions of jet pumps through a methodology that predicts the pressure loss of the fluid in overexpanded and underexpanded using CFD simulations; It was concluded that an adequate control of the primary pressure and the nozzle throat area can avoid the undesirable blockage condition.

One of the most important applications of jet_pumps is for refrigeration and air conditioning systems. For example, [8] used ANSYS Fluent to simulate fluid flow in a variable area jet pump for refrigeration systems and compared its performance to a conventional constant area jet_pump, noting a 40% pressure ratio increase. On the other hand, [9] studied the influence of the throat and divergent length of a refrigeration jet pump on its performance using ANSYS Fluent, obtaining optimum values of 0.338 m and 0.844 m, respectively, for suction or secondary pressure of -100.288 kPa. [10] developed an optimization model for the jet pump efficiency in terms of the ratio between the area of the constant section of the mixing chamber and the nozzle throat area, whereas [11] carried out an experimental study about the influence of the throat area of the primary nozzle on the jet pump performance in an ejector cooler R141b. Another author [12] found that the change in the length of the constant section of the diffuser in jet pumps used for cooling does not have a relevant influence on the drag coefficient, but it does on the increase in the back pressure of the mixture.

The efficiency of the jet pump depends on its geometry, and several works have focused on parametric analyzes and optimizations of the geometry of the jet pump. For example, [13] developed a geometric optimization of a jet pump using CFD software, where the k-ε turbulence model was used due to its ability to accurately predict jet pump performance parameters, such as the ratio of pressure, drag coefficient, and energy efficiency, without involving a high computational cost.

An increase of the jet pump performance from 29% to 33% was achieved, with a consequent reduction of the energy consumption of 20%. Similarly,[14] used the k-ε turbulence model to study the influence of some transient phenomena on the jet pump performance, finding that some vortical structures separated from the secondary flow can bring about the reduction of the drag coefficient. Four different turbulence models (k-ε realizable, k-ε standard, RSM y SST) were used by [15] to estimate the optimal area ratio to maximize the energy efficiency, obtaining an optimum value of 4.61 with a corresponding maximum efficiency of 38.46%. On the other hand, [16] estimated the appropriate values of the constants of the standard model of turbulence K-ε for a jet fuel pump. As can be seen, the k-ε model is widely used in fluid dynamic simulations of jet pumps, and this is also used in this work.

Orozco, 2022 [6], co-author of this work, developed a one-dimensional analytical model to obtain the most suitable dimensions and geometry of a jet pump for vacuum distillation applications of ethanol, which allows finding the ideal throat diameter of the nozzle, among other parameters, to generate a vacuum pressure of 8 kPa in the secondary port for the distillation of ethanol at room temperature. This model was compared with the CFD simulations in [12], obtaining similar results for the coincidence number, the fluid pressure and the fluid velocity in the longitudinal direction of the jet pump, although with important differences in some local variables. In said work [12], the influence of the combination of the inlet pressure and the position of the main nozzle on the performance of the jet pump was also studied. The optimization of some non-dimensional geometrical parameters of the jet pump to pressure ratio, maximize the drag coefficient, and energy efficiency was performed in [6], identifying the ratio of the nozzle inlet area to the nozzle throat area, which is the parameter considered in the present

work, as the most influential parameter. Bearing this in mind, this work is devoted to developing a parametric study about the influence of the area ratio (AR) on the performance of jet pumps (as quantified by the drag coefficient, pressure ratio, and energy efficiency) for vacuum distillation applications. The influence of this important non-dimensional parameter (AR) on the Mach number contours and profiles, as well as in the velocity vector field, is analyzed too.

The performance parameters considered here have been previously used in published literature [2]; [3]; [4]; [5] and can be defined as follows:

Drag coefficient: this parameter is extensively used to account for the jet pump performance. It is defined as the ratio of the mass flow rate at the secondary port, ms, to the mass flow rate at the primary one, mp, as given by (1).

$$C_d = \frac{\dot{m}_s}{\dot{m}_p}$$
(1)

Pressure ratio: this parameter accounts for the pressure recovery from the secondary (suction) to the outlet (discharge) port (Pd-Ps) concerning the global pressure gradient between the primary (inlet) and outlet (discharge) port (Pp-Pd), as shown in (2).

$$PR = \frac{P_d - P_s}{P_p - P_d}$$
(2)

Energy efficiency: It can be defined as the ratio of the power delivered to the secondary (suction) fluid to the power lost by the primary (inlet) fluid. In incompressible fluids, energy efficiency can be obtained as the product of the drag coefficient (Cd) and the pressure ratio (PR) [6]. Since a compressible, ideal gas is considered here, this simplification is not valid and the (3) shall be used instead:

$$\eta = \frac{\dot{m}_s(e_d - e_s)}{\dot{m}_p(e_p - e_d)}$$
(3)

Where:
ed: Specific energy at the outlet or discharge port,
es: Specific energy at the secondary or suction port,
ep: Specific energy at the primary or inlet port.

II. METHODOLOGY

The numerical methodology used here was previously implemented and validated with experiments in [12], and the principal features of this methodology are summarized hereunder.

A. Computational domain and mesh

The computational space is as appeared in Fig. 2a and Fig. 2b, where it can be noticed that a half geometry of the jet pump is considered; the principal measures are presented, with a changeable inlet diameter to modify the area ratio (AR).
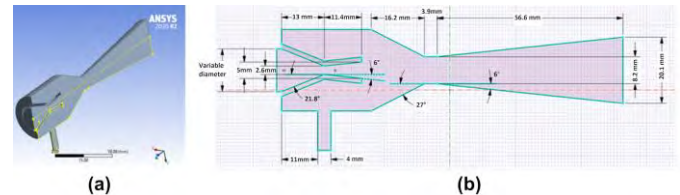

Fig. 2. a) 3D model of jet pump, b) Principal dimensions of the jet pump [12]

Linear tetrahedral (Tet4) and wedge (Wed6) elements are used to mesh the computational domain. The definitive mesh size is determined by means of a mesh-dependency analysis, deeming the three performance parameters of the present work, namely, drag coefficient (Cd), pressure ratio (PR), and energy efficiency (η). A global size for the whole physic domain is considered, with local mesh improvement in the nozzle walls employing elements two times smaller than the global size and an inflation operation with a transition ratio of 0.6 and a growth rate of 1.1. The variation of Cd, PR, and η, as well as of the computational time, with the number of nodes can be observed in Fig. 3, where meshes with different global sizes are taken into account: 1 mm global (51141 nodes), 0.8 mm global (81348 nodes), 0.6 mm global (147504 nodes), 0.4 mm global (360110 nodes), 0.3 mm global (652693 nodes) and 0.2 mm global (1585785 nodes). In the present work, a global mesh size of 0.4 mm was selected (see filled markers in Fig. 3). Finer meshes lead to an important rise in the computational time with insignificant changes in the performance parameters (Cd, PR, and η). For instance, variation of these parameters when global mesh size changes from 0.4 mm to 0.3 mm are 0.4%, 1.0%, and 1.1%, respectively, with an increasing in the computational time of 110%. The final mesh used in the present work is shown in Fig. 4.
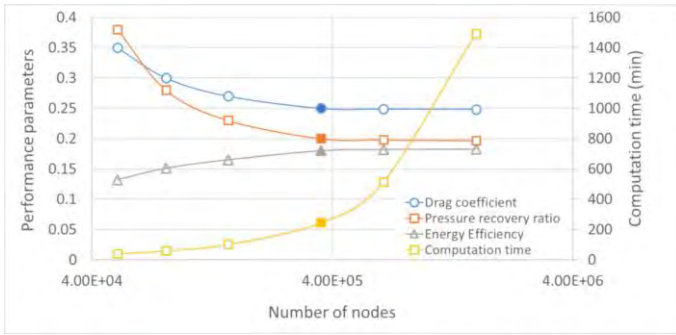
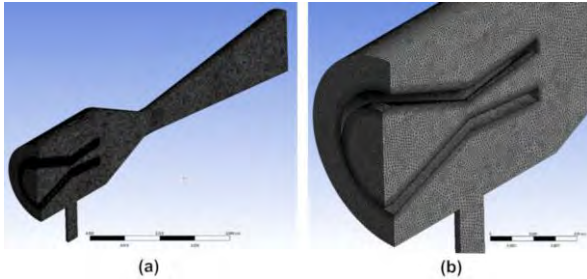Fig. 3. Results of mesh-dependency analysis and computation time.

Fig. 4. Definitive mesh (0.4 mm global size). a) General view, b) Detail view of inflation

The mesh-dependency analysis is complemented using the Grid Converge Index (GCI) technique [17], [18]; which is based on the Richardson extrapolation and allows quantifying the convergence level of the numerical solution. For the six mesh-sizes represented in Fig. 3, the refinement constant between two consecutive meshes, c_{ref}, is computed considering the global mesh-size, whereas a constant safety factor of $F_s = 1.25$ is deemed. In the GCI technique, for any three consecutive meshes, represented as u, v, w from the coarser to the finer one, the Grid Convergence Index for the intermediate mesh (v) can be computed as follows [18]:

$$GCI_v = \frac{GCI_{uv}}{c_{ref}{}^p . GCI_{vw}} \qquad (4)$$

Where GCI_{uv}, GCI_{vw} and p represent the Grid Convergence Index between meshes u and v, Grid Convergence Index between meshes v and w, and the convergence order, as defined by:

$$GCI_{uv} = \frac{F_s . \frac{(f_u - f_v)}{f_v}}{c_{ref}{}^p - 1} \qquad (5)$$

$$GCI_{vw} = \frac{F_s . \frac{(f_v - f_w)}{f_w}}{c_{ref}{}^p - 1} \qquad (6)$$

$$p = \frac{ln\left(\frac{f_u - f_v}{f_v - f_w}\right)}{ln(c_{ref})} \qquad (7)$$

With f_u, f_v and f_w as the convergence parameters (C_d, PR and η) for the course, medium and fine mesh, respectively. The numerical solution is within the asymptotic range of convergence when GCI_v is close to 1. Fig. 5 represents the change of Grid Convergence Index (GCI) for the meshes 2 to 5.

Where it can be confirmed that the global mesh size of 0.4 mm is suitable in the present work since the Grid convergence Index (GCI) is very close to 1 for all convergence parameters (C_d, PR and η).
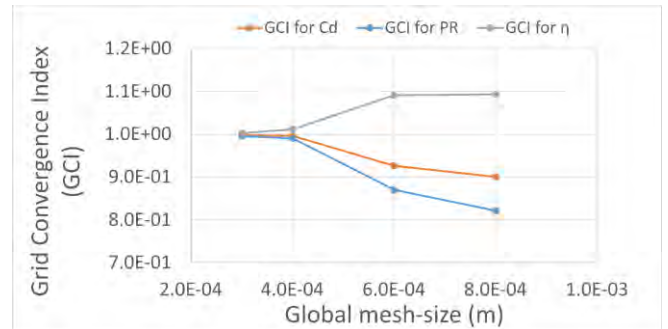

Fig. 5. Grid Convergence Index (GCI) for the convergence parameters (C_d, PR and η)

The histogram of skewness of the mesh elements is shown in Fig. 6. According to [6], skewness of excellent quality elements ranges between 0 and 0.25, good quality elements between 0.25 and 0.50, and moderate-quality elements between 0.50 and 0.75. As can be appreciated in Fig. 6, most of the elements lie in those ranges, denoting an acceptable mesh quality.
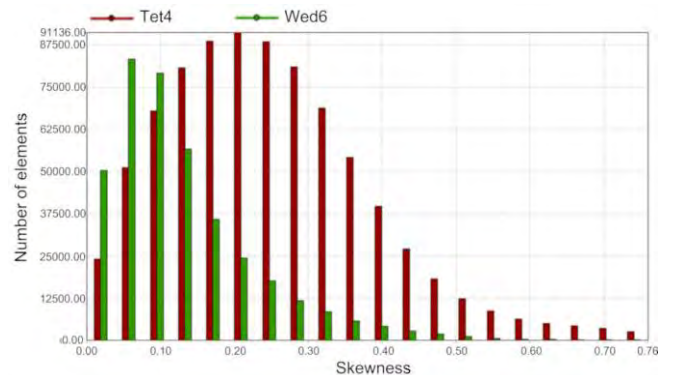

Fig. 6. Histogram of skewness of mesh elements.

B. Computational setup

As formerly mentioned, ANSYS Fluent is used here to carry out the CFD simulations of the jet pump. Therefore, the finite volume method is implemented and seven governing equations are solved for each control volume (mass, momentum in x, y, and z, energy, and two turbulence equations). According to previous works [6], [12], the k-ε turbulence model is very suitable for fluid flow simulations in jet pumps, and this is the model deemed here. Accordingly, two conservation equations are solved for the turbulence modeling:

Conservation equation (8) for the turbulent kinetic energy, κ:

$$\frac{\partial}{\partial t}(\rho k) + \frac{\partial}{\partial x_i}(\rho k u_i) = \frac{\partial}{\partial x_j}\left[(\mu + \frac{\mu_t}{\sigma_k})\frac{\partial}{\partial x_j}(k)\right] +$$
$$G_k + G_b - \rho\varepsilon - Y_M + S_K \tag{8}$$

Conservation equation (9) for the turbulent dissipation rate, ε:

$$\frac{\partial}{\partial t}(p\varepsilon) + \frac{\partial}{\partial x_i}(\rho\varepsilon u_i) = \frac{\partial}{\partial x_j}\left[(\mu + \frac{\mu_t}{\sigma_\varepsilon})\frac{\partial}{\partial x_j}(\varepsilon)\right] +$$
$$C_{1\varepsilon}\frac{\varepsilon}{k}(G_k + C_{3\varepsilon}G_b) - C_{2\varepsilon}\rho\frac{\varepsilon^2}{k} + S_\varepsilon \tag{9}$$

Where the turbulent viscosity is calculated as follows

$$u_t = \rho C\mu\frac{k^2}{\varepsilon}$$

In the present work, fluid is air, which is governed by the ideal gas law and has the properties presented in Table 1. The activation of the compressibility correction of ANSYS Fluent is convenient here because the fluid is compressible and flow can be supersonic in some zones of the domain; this allows considering the contribution of fluctuating dilatation to the overall dissipation rate, Y_M. The parameters of the k-ε turbulence model used here are shown in Table 2.

TABLE 1
STROUHAL NUMBER FOR DIFFERENT GEOMETRIC CASES

Property	Value and units
Specific Heat (Cp)	1006.43 J/kg.
Thermal conductivity (K)	0.0242 W/my

Dynamic viscosity (μ)	1.79E-05 gums
Molecular Weight (Mw)	28.96 g/mol

TABLE 2
CONSTANTS OF THE K-E TURBULENCE MODEL

Symbol	Value
Ch	0.09
C1ε	1.44
C2ε	1.92
σκ	1.0
σε	1.3
Prt	0.85

Following a recently published work [15], the Enhanced Wall Treatment method is considered to relate the solution variables in cells adjacent to walls with the corresponding variables of the walls. To guarantee the location of the first cell in the log-layer, it is recommended to keep the dimensionless wall distance of this cell, y+, between 30 and 300. For the inflation mesh represented in Fig. 4, y+ for the first cell ranges between 62 and 85 in all simulations considered here, complying this; additionally, the inflation controls (growth rate, transition ratio and number of layers) allow a smooth transition between the wedge inflation mesh and the tetrahedral one.

In addition to the classical convergence monitors used in this kind of problem (continuity, velocity in x, y, and z, energy, turbulent kinetic energy, and turbulent dissipation rate), the three performance parameters considered here (Cd, PR, η) are monitored during the simulation as well, specifying permissible residuals of 1x10-6 as convergence criteria.

The initialization of the numerical solution is done with a hybrid scheme with 20 iterations and the default turbulence parameters. The principal characteristics of the solver are shown in Table 3.

TABLE 3
PRINCIPAL CHARACTERISTICS OF THE SOLVER

Characteristic of the	Option
Solution scheme	Coupled pressure-

Spatial discretization	Second Order Upwind
Gradient calculation	Least-squares based
Relaxation factor for	0.5
Relaxation factor for momentum	0.5
Relaxation factor for	1
Relaxation factor for	1
Relaxation factor for turbulent	0.75
Relaxation factor for turbulent dissipation	1
Relaxation factor for energy	0.75

C. Boundary conditions

The boundary conditions of this problem are shown in Table 4, where the boundary region, condition type, value, and characteristics are identified. The boundary regions are shown in Fig. 7.

TABLE 4
SUMMARY OF THE BOUNDARY CONDITIONS

Boundary Region	Condition Type	Value/Characteristics
Primary port	Gauge pressure	55 kPa @298 K, Pressure at laboratory scale. Manometer Features: Pressure Transducer Sensor 1/4 inch, 5V, 0 – 1200 kPa, at the compressor outlet. Prevent Reverse Flow is activated in the inlet boundary condition.
Secondary port	Absolute pressure	8 kPa @295 K Pressure for azeotropic distillation of ethanol at ambient temperature Prevent Reverse Flow is activated
Outlet port	Initial gauge pressure	4.5 kPa This pressure continuously changes as the simulation is executed.
Longitudinal plane	Symmetry condition	Non-flux, zero shear stress

External walls	Wall condition	No penetration, no-slip, stationary
Internal walls	Wall condition	No penetration, no-slip, stationary

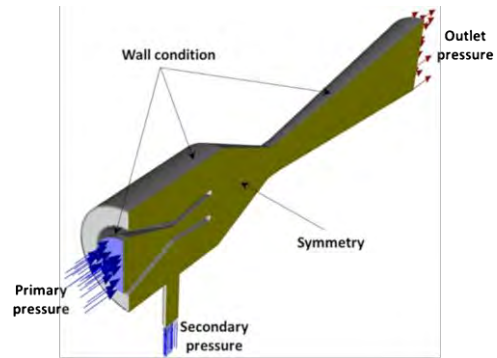Fig. 7. Boundary conditions of the jet pump

III. SIMULATION RESULTS

Fig. 1 shows the ideal operation of a jet pump. According to [2] and [13], when the driving fluid reaches sonic speed in the nozzle throat (point 1), supersonic speed will be obtained at the nozzle outlet (point 2), as long as suitable area ratios between inlet, throat, and outlet of the nozzle are present; in such a case, the greatest pressure drop will be obtained in ideal working conditions, as well as the highest drag coefficient, Cd, is this the best-operating conditions for the pump. Similarly, Fig. 1 shows the primary and secondary fluids involved in the process and their behavior throughout the device.

In the present work, it is studied the influence of AR on the drag coefficient (Cd), pressure ratio (PR), Energy Efficiency (η), and maximum Mach number (Ma, max). In Table 5, the change of these parameters with the area ratio (AR) can be observed, with Cd, PR, and Ma, max as the sensitive parameters to the change of AR, whereas the energy efficiency (η) is not significantly affected for these particular geometric and operating conditions. Parameters Cd and PR continuously increase with AR, whereas the variation of Ma, max with AR is non-monotonic. Since larger values of performance parameters Cd and PR are obtained for the larger area ratio (AR=30), it can be inferred that the best performance of the jet pump occurs for such a ratio; despite the maximum Mach number, Ma, max, is not the greatest for such ratio (AR=30), it is larger than

1 (supersonic flow after nozzle outlet), which is by the normal working of the jet pump (see Fig. 1).

CASE STUDIES	AR	Cd	PR	η	Ma, max
1	10	0.221	0.022	0.224	5.075e+00
2	15	0.238	0.033	0.230	4.818e+00
3	20	0.245	0.039	0.235	4.721e+00
4	25	0.248	0.052	0.240	4.903e+00
5	30	0.250	0.058	0.233	4.538e+00

Figs 8, 9, and 10 represent the Mach number contours, Mach number profiles along with the longitudinal directions, and field of velocity vectors for all cases of AR considered, respectively. As can be observed in Figs. 8 and 9, several peaks of Mach numbers can be appreciated in the mixing chamber, before the fluid flow enters the diffuser throat. This behavior of Ma takes place because, in this chamber, the mixing between primary and secondary fluids is not homogenized; in general, a suitable homogenization is obtained once the fluid flow passes through the diffuser throat [12], as can be confirmed in fig. 9 for all cases. The sharp reduction of Ma in those peaks is associated with the formation of shock waves. In all cases considered here, despite the abrupt reduction of Ma, especially in the peaks of the first, fluid flow remains supersonic just after the peak (Ma>1), as can be seen in Figs. 8 and 9, which allows inferring that shock waves are oblique [27]. This statement can be confirmed in Fig. 9, where it can be noticed that in the longitudinal positions corresponding to the peaks of Ma, notorious changes in the direction of velocity vectors can be appreciated, which is proper of the oblique shock waves [12].
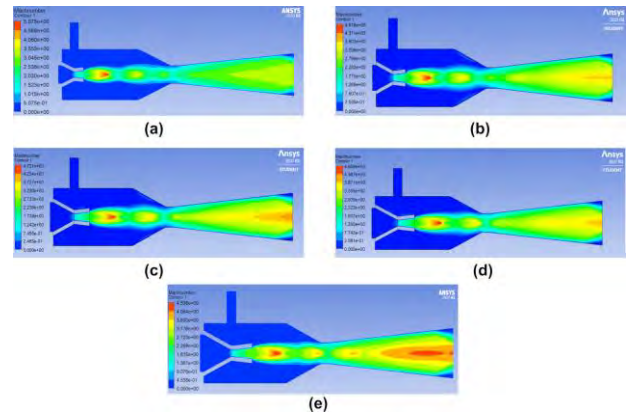

Fig. 8. Mach number contours for all cases of AR. a) AR=10, b) AR=15, c) AR=20, d) AR=25, e) AR=30.
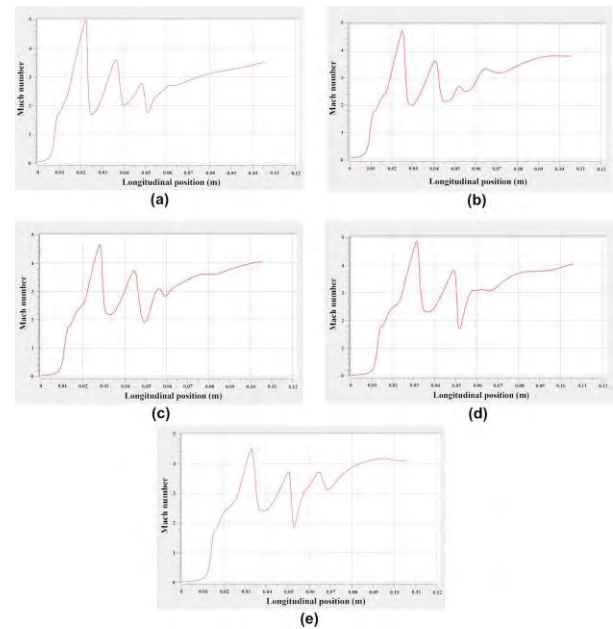

Fig. 9. Mach number profile along the longitudinal direction for all cases of AR. a) AR=10, b) AR=15, c) AR=20, d) AR=25, e) AR=30.
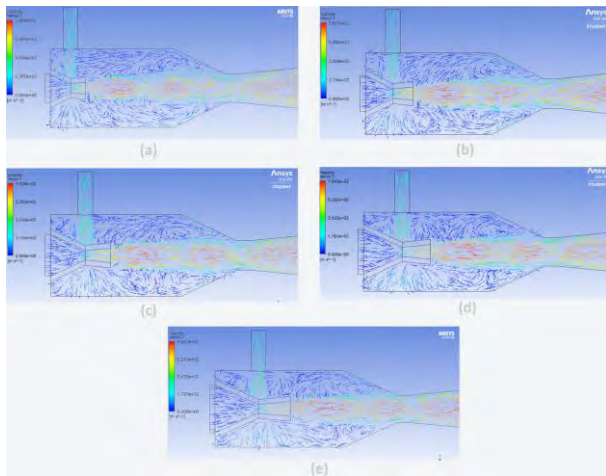
Fig. 10. Field of velocity vectors for all cases of AR.a) AR=10, b) AR=15, c) AR=20, d) AR=25, e) AR=30.

IV. CONCLUSIONS

Computational Fluid Dynamics (CFD) was used in the present work to study the influence of the ratio of the inlet to nozzle throat areas (AR) on the performance of a jet pump used for vacuum distillation of ethanol. Results show that drag coefficient (Cd), pressure ratio (PR), and maximum Mach number (Ma, max) are influenced by AR, whereas the energy efficiency (η) is not considerably affected for these particular geometric and operating conditions. The best performance of the jet pump is achieved for the maximum ratio, AR=30.

Additionally, results of Mach number contours, Mach number profiles along with the longitudinal directions, and field of velocity vectors allow inferring the arising of oblique shock waves in the mixing chamber where primary and secondary fluids are not fully homogenized. This is present for all values of AR, bringing about a change in the direction of velocity vectors; however, the fluid flow remains supersonic from the nozzle outlet to the diffuser outlet, which is beneficial for the jet pump performance.

The application of CFD in the study of the jet pump allowed identifying the fluid flow behavior and quantifying the jet pump performance in terms of Cd, PR, and η, demonstrating the importance of using CFD in the design and/or evaluation of jet pumps.

REFERENCES

[1] A. B. A. Arbab, "Simulation of Ejector Flow Behavior Which Produce Vacuum in Power Plants Condenser," *Doctoral dissertation Sudan University of Science and Technology*, 2018.

[2] J. Chen, H. Havtun, and B. Palm, "Investigation of ejectors in refrigeration system: Optimum performance evaluation and ejector area ratios perspectives," *Applied Thermal Engineering*, vol. 64, no. 1–2, pp. 182–191, Mar. 2014, doi: 10.1016/j.applthermaleng.2013.12.034.

[3] T. Thongtip and S. Aphornratana, "An experimental analysis of the impact of primary nozzle geometries on the ejector performance used in R141b ejector refrigerator," *Applied Thermal Engineering*, vol. 110, pp. 89–101, 2017, doi: 10.1016/j.applthermaleng.2016.08.100.

[4] X.-D. Wang and J.-L. Dong, "Numerical study on the performances of steam-jet vacuum pump at different operating conditions," *Vacuum*, vol. 84, no. 11, pp. 1341–1346, 2010.

[5] R. Yapici and K. Aldaş, "Optimization of water jet pumps using numerical simulation," *Proceedings of the Institution of Mechanical Engineers, Part A: Journal of Power and Energy*, vol. 227, no. 4, pp. 438–449, 2013, doi: 10.1177/0957650913487529.

[6] W. Orozco, I. D. P. Arcila, and J. A. Palacio-Fernández, "Geometric Optimization of Jet Pump Used in Vacuum Distillation Applications under Different Operating Conditions using Genetic-algorithm Methods," *Journal of Applied and Computational Mechanics*, vol. 8, no. 1, pp. 340–358, 2022, doi: 10.22055/jacm.2021.38411.3228.

[7] S. Varga, A. C. Oliveira, X. Ma, S. A. Omer, W. Zhang, and S. B. Riffat, "Experimental and numerical analysis of a variable area ratio steam ejector," *International Journal of Refrigeration*, vol. 34, no. 7, pp. 1668–1675, 2011, doi: 10.1016/j.ijrefrig.2010.12.020.

[8] E. Rusly, L. Aye, W. W. S. Charters, and A. Ooi, "CFD analysis of ejector in a combined ejector cooling system," *International Journal of Refrigeration*, vol. 28, no. 7, pp.

1092–1101, 2005, doi: 10.1016/j.ijrefrig.2005.02.005.

[9] T. Sriveerakul, S. Aphornratana, and K. Chunnanond, "Performance prediction of steam ejector using computational fluid dynamics: Part 1. Validation of the CFD results," *International Journal of Thermal Sciences*, vol. 46, no. 8, pp. 812–822, 2007.

[10] B. J. Huang and J. M. Chang, "Empirical correlation for ejector designCorrélation empirique pour la conception des éjecteurs," *International Journal of Refrigeration*, vol. 22, no. 5, pp. 379–388, 1999.

[11] "ANSYS FLUENT 12.0 Theory Guide - 4.4.2 RNG - Model," 2009. https://www.afs.enea.it/project/neptunius/docs/fluent/html/th/node59.htm (accessed Jan. 23, 2020).

[12] W. Orozco, J. A. Palacio-Fernandez, I. D. P. Arcila, J. S. Z. Monsalve, and J. A. H. Isaza, "Analysis of a Jet Pump Performance under Different Primary Nozzle Positions and Inlet Pressures using two Approaches: One Dimensional Analytical Model and Three Dimensional CFD Simulations," *Journal of Applied and Computational Mechanics*, vol. 6, no. Special Issue, pp. 1228–1244, 2020, doi: 10.22055/JACM.2020.33339.2205.

[13] H. El-Dessouky, H. Ettouney, I. Alatiqi, and G. Al-Nuwaibit, "Evaluation of steam jet ejectors," *Chemical Engineering and Processing: Process Intensification*, vol. 41, no. 6, pp. 551–561, 2002.

[14] G. Besagni, "Ejectors on the cutting edge: The past, the present and the perspective," *Energy*, vol. 170, pp. 998–1003, Mar. 2019, doi: 10.1016/j.energy.2018.12.214.

[15] Ansys, "ANSYS Meshing User' s Guide," no. January, 2022.

[16] F. M. White, *Fluid mechanics*, 7th ed. New York, 2011.

[17] N. Baker, G. Kelly, P. O'Sullivan. "A grid convergence index study of mesh style effect on the accuracy of the numerical results for an indoor airflow profile" International Journal of Ventilation 19(4),sept. 2020. doi:10.1080/14733315.2019.1667558

[18] M. Rakowitz. "Grid Refinement Study with a UHCA Wing-Body Configuration Using Richardson Extrapolation and Grid Convergence Index GCI," Gennan Aerospace Center (DLR), Institute of Design Aerodynamics, Lilienthalplatz 7, 38108 Braunschweig, Germany, 2002.